Low-Temperature Oxidation of Nitrided Iron Surfaces

Jessica Torres,[†] C. C. Perry,[†] Stephen J. Bransfield,[†] and D. Howard Fairbrother*[,†,‡]

Department of Chemistry and Department of Materials Science and Engineering, The Johns Hopkins University, 3400 North Charles Street, Baltimore, Maryland 21218

Received: December 22, 2002; In Final Form: April 8, 2003

The low-temperature (<150 K) oxidation of nitrided iron surfaces exposed to oxygen and water was probed using X-ray photoelectron spectroscopy (XPS), reflection absorption infrared spectroscopy (RAIRS), and mass spectrometry (MS). During exposure of nitrided iron surfaces to oxygen, iron oxynitride ($Fe_xN_yO_z$), nitrosonium ions (NO^+), as well as nitrite/nitrito- and nitrate-type species were observed. The production of nitrite/nitrito and nitrate species is taken as evidence for the existence of oxygen insertion chemistry into the iron nitride lattice under these low-temperature oxidation conditions. No molecular nitrogen was produced during reactions with oxygen or water in contrast to oxidation studies on other transition metal nitrides. Upon annealing the oxidized overlayer, nitrogen desorbs exclusively as nitric oxide (NO) between 250 and 400 K. In contrast to oxygen, the reactivity of nitrided iron surfaces toward water was limited to the production of adsorbed N−O species.

Introduction

Transition metal nitride coatings have found numerous industrial applications as a result of their unique combination of physical and chemical characteristics, including extreme hardness,[1,2] biocompatibility,[3] as well as oxidation and wear resistance.[1,2] For example, TiN, ZrN, and HfN are utilized as optoelectronic coatings,[4] while TiN and CrN coatings are used in the tool industry.[1,5] TiN is also often employed as a barrier layer to inhibit Cu diffusion in copper-based metal interconnects,[6] while iron nitrides in their many phases are widely used as coatings for magnetic and optical recording media.[2]

Although nitrides are thermodynamically stable in extreme chemical and thermal environments, they are susceptible to surface oxidation. Thus, oxidation of transition metal nitrides has been shown to produce metal oxides and a complex array of nitrogen-containing species, whose presence can modify both the physical and chemical characteristics of the interfacial region. As a result, a number of scientific investigations have been directed toward understanding the mechanisms and product distributions associated with nitride oxidation processes. For example, X-ray photoelectron spectroscopy (XPS) studies on CrN,[7,8] TiN,[8,9] and ZrN[9] surfaces following oxidation under both ambient and high-temperature conditions, as well as after electrochemical oxidation have hypothesized that interstitial N_2 is produced at the oxide−nitride interface. In addition to molecular nitrogen, oxynitrides have also been identified during the air oxidation of TiN,[10] the thermal oxidation of TiN[9] and ZrN,[9,11] and during the electrochemical oxidation of ZrN,[9,12] although there is widespread disagreement in the literature regarding N(1s) peak assignments. The complexity of the nitride oxidation process is highlighted by the fact that in TiN[8,9] and ZrN,[9,12] both interstitial N_2 and oxynitrides are identified as reaction products.

Despite its importance in the magnetic and recording industries, the oxidation of iron nitrides has received little attention.[13,14] Furthermore, in the limited number of studies on iron nitride oxidation, no consensus has emerged regarding the nature of the surface species produced. Graat et al.,[14] in a study on the effects of O_2-oxidation (8×10^{-5} Pa, 323 to 573 K) on ϵ-Fe_2N_{1-x}, reported the appearance of an XPS peak in the N(1s) region at a lower binding energy than the parent nitride peak. Angle-resolved XPS measurements showed that this peak was located closer to the substrate−oxide interface than the underlying nitride. In contrast, a separate study on the O_2 plasma and air oxidation of γ'-Fe_4N and ϵ-$Fe_{2-3}N$ by Cocke et al.[13] observed the formation of a N(1s) peak at a higher binding energy than the parent nitride peak, which they attributed to an oxidized nitrogen (NO_x) species.

This study describes the oxidation of nitrided iron surfaces by oxygen and water under vacuum conditions at low temperatures (<150 K) with a focus on the nitrogen-containing species produced and their thermal stability. At low reaction temperatures, new pathways and intermediates have been identified using a number of complimentary *in-situ* surface analytical techniques. In addition, the controlled UHV environment has facilitated a comparison of the differences between nitride oxidation during exposure to the two major oxidizing agents present under ambient or high temperature conditions: water and oxygen. The results from our study indicate that the initial exposure of nitrided iron surfaces to oxygen results in the formation of nitrite/nitrito species, nitrosonium ions, oxynitrides, and iron oxide(hydroxide). Upon prolonged oxygen exposures, nitrate species are observed in the oxidized overlayer, indicative of an O-insertion mechanism into the iron nitride lattice, a process that has not been observed in previous studies of nitride oxidation. Upon annealing above 250 K, nitrogen desorbs from this oxidized nitride overlayer as NO. A comparison between the reaction products observed during oxygen and water adsorption highlights the lower oxidizing power of water.

Experimental Section

Experiments were performed in two different ultrahigh vacuum (UHV) chambers. The first UHV chamber, where the majority of the experiments reported in this study were carried out, was equipped with a PHI ESCA 5400 XPS system ($P_{base} \approx 5 \times 10^{-9}$ Torr) and a Balzers Prisma quadrupole mass

* Author to whom correspondence should be addressed.
[†] Department of Chemistry.
[‡] Department of Materials Science and Engineering.

10.1021/jp027802w CCC: $25.00
Published on Web 05/15/2003

spectrometer for thermal desorption experiments (chamber-1). The second UHV chamber ($P_{base} \approx 3 \times 10^{-8}$ Torr) was equipped with capabilities for reflection absorption infrared spectroscopy (RAIRS), XPS (PHI ESCA 5100 system), and residual gas analysis (Stanford Research Instruments, SRS 200) (chamber-2).

All XP spectra were collected using Mg Kα incident irradiation (1253.6 eV) at a takeoff angle of 45° from the sample normal. In chamber-1, elemental scans used a pass energy of 44.75 and 0.125 eV/step, while in chamber-2 a pass energy of 89.45 and 0.25 eV/step was employed. XPS data fitting was performed using Shirley background subtraction and 100% Gaussian peaks with the FWHMs constrained between 1.6 and 1.8 eV. RAIRS measurements were carried out using a Mattson Infinity Series FTIR spectrometer equipped with external beam capabilities. Experiments carried out in this investigation employed indium antimonide (InSb) (1900 cm^{-1}−4000 cm^{-1}) and narrow-band mercury−cadmium−telluride (MCT) (700 cm^{-1}−4000 cm^{-1}) detectors. RAIR spectra were recorded at a resolution of 4 cm^{-1} by summing 500 scans. Scans were referenced to the nitrided iron surface before oxidation. Desorption experiments were carried out in chamber-1 by placing the oxidized surfaces in front of the mass spectrometer (sample-to-ionizer distance ≈ 2.5 cm). Substrate heating was accomplished by passing AC current through the sample using an external power supply; an average 3 K/s temperature ramp was maintained during substrate annealing.

Sample Mounting. Substrates were mounted on dedicated UHV manipulators (McAllister Technical Services) with capabilities for precision *xyz* translation, rotation, and sample cooling as well as direct sample heating. In chamber-1, polycrystalline iron samples were mounted onto a tantalum foil that was spot-welded via copper rods to a ceramic feed-through coupled to a UHV manipulator, as previously described.[15] In chamber-2, an iron mirror (1 cm diameter) was spot welded via Ta strips onto the copper rods. In both chambers, samples were cooled by passing liquid nitrogen into a hollow stainless steel tube connected to the ceramic feed-through. The sample temperature was monitored using a chromel−alumel thermocouple spot-welded to the back of the tantalum foil in chamber-1 and spot welded to the back of the Fe mirror in chamber-2. This cooling arrangement allowed sample temperatures of <150 K to be maintained in each system.

Synthesis of Nitrided Iron Surfaces. In chamber-1, nitrided iron films were synthesized by exposing the polycrystalline iron samples to the N_2^+ and N^+ ions generated by passing molecular nitrogen through a Physical Electronics 04-303 ion gun operating at 20 mA emission current and beam energy of 3 keV for approximately 30 min. In chamber-2, the same conditions were employed using a Physical Electronics 04-300 ion gun. After ion implantation, the nitrogen concentration determined by XPS was typically between 20 and 40%, while the O concentration was <1%. A variety of different nitride phases can be formed, depending upon the experimental conditions. A survey of the literature related to the synthesis of iron nitrides using ion energies (2−5 keV) comparable to those employed in the present investigation suggests that the dominant nitride phase is probably $Fe_{16}N_2$.[16]

An iron(III) nitrate standard ($Fe(NO_3)_3 \cdot 9H_2O$, 98% purity—Alfa Aesar) was employed for XPS analysis. To remove the water of hydration, it was necessary to pump the compound overnight in the entry-lock of chamber-1 prior to XPS analysis.

O/O_2 Source. Atomic oxygen was generated using a Thermal Gas Cracker TC-50 (Oxford Applied Research). This gas cracker works by dissociating molecular gases such as oxygen into a stream of atomic, low-energy reactive species as described in a previous publication.[17] In both UHV systems, the O/O_2 source was located in line-of-sight with the sample (target-to-sample distance ≈ 5 cm), operated at 40 W. It should be noted that throughout this study, all oxygen exposures were carried out at $6(\pm 1) \times 10^{-7}$ Torr. XPS results indicate that oxidation with atomic or molecular oxygen gave the same reaction products, although by employing a mixture of O/O_2 species, the reaction rate was increased due to the greater reactivity of atomic oxygen. The purity of isotopically labeled $^{18}O_2$ (Icon Isotopes $^{18}O_2$ 99%) used in this study was verified independently by mass spectrometry.

Results

Figure 1 shows the variation in the normalized N(1s) XPS region of nitrided iron surfaces (held at a temperature <150 K) as a function of oxygen exposure. Figure 1 illustrates that low-temperature exposure of nitrided iron to oxygen is a complex process evidenced by significant changes in the N(1s) XPS region, indicating the production of a wide range of new nitrogen-containing species. Figure 2a−c shows the variation in the relative concentration for the various fitted N(1s) peaks as a function of oxygen exposure time. Figure 2d shows the change in elemental composition of the nitrided overlayer based on the variation in the total nitrogen XPS area, as well as the fitted O^{2-} and H_2O XPS areas (measured from analysis of the O(1s) area—see for example Figure 5) as a function of increasing oxygen exposure. Hydroxyl species were also evidenced in the O(1s) region, although their dependence was qualitatively similar to that of O^{2-} and they have been omitted for the sake of clarity.

Before oxygen exposure, the N(1s) region exhibits a single peak located at 397.4 eV (Figure 1a), whose peak position and line shape are consistent with the presence of iron nitride.[13,14,18] During the early stages of oxidation (t < 20 min), the iron nitride peak decreased in intensity to approximately 50% of its initial value (Figure 2a) while the spectral intensity in the N(1s) region between 402 and 395 eV broadens considerably (Figure 1b,c). The N(1s) spectral envelope between 402 and 395 eV could be well fit by the inclusion of three new peaks centered at 396.1, 399.4, and 400.9 eV in addition to the original iron nitride peak at 397.4 eV; however, the N(1s) peak at 400.9 eV is only a minor component of the overall N(1s) spectral envelope. A new peak is also evident at even higher binding energies in the N(1s) XPS region during the early stages of oxidation, centered at 402.9 eV. For oxidation times greater than 20 min, only small changes in the area of the peaks at 396.1 and 399.4 eV were observed, while the peak at 400.9 eV increases in intensity (Figures 1c−e and 2a,b). A new peak at 406.4 eV also appears in the N(1s) region and becomes increasingly prominent for prolonged oxidation times, while the peak at 402.9 eV decreased in relative intensity. The effect of oxygen exposure on the N(1s) region is highlighted by the N(1s) difference spectrum shown in Figure 1f for a nitrided iron surface exposed to oxygen for 180 min referenced to a nitrided iron surface prior to oxidation. The N(1s) difference spectrum shows a large negative peak at ≈397.4 eV, indicative of the loss of native iron nitride species. In contrast, positive features are observed at distinct peaks centered at 396.1 and 406.4 eV as well as a broader component between 399 and 402 eV.

Figure 2d shows that the formation of iron oxide(hydroxide) during the oxidation process, evidenced by production of the O^{2-} and OH^- species as well as Fe^{2+}/Fe^{3+} in the Fe(2p) region (see Figure 5), is essentially complete after ≈20 min. In contrast

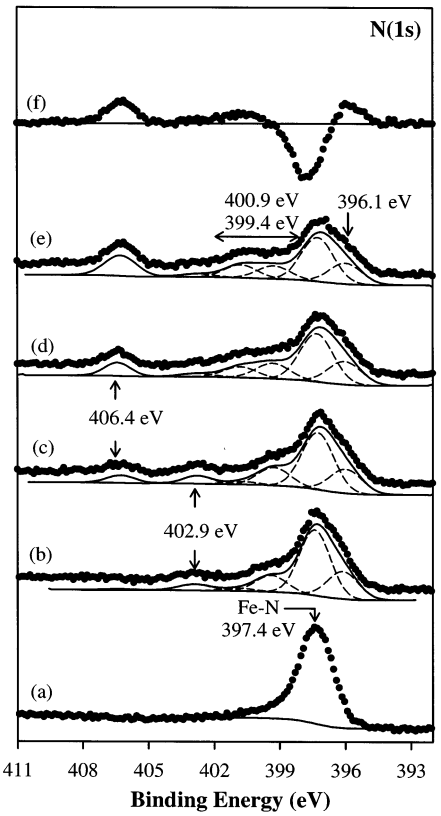

Figure 1. Variation in the N(1s) XPS region of a nitrided iron surface (a) before oxygen exposure and after (b) 10, (c) 20, (d) 60, and (e) 180 min of oxygen exposure with the substrate held <150 K. Raw XPS spectra are shown as filled circles, peak fits as dashed lines, and envelopes and backgrounds as solid lines. (f) This figure corresponds to the difference spectra between the normalized N(1s) regions before oxidation and after 180 min of oxygen exposure. Each experiment was carried out on a freshly nitrided surface in order to minimize the effects of X-ray degradation during data acquisition (Figure 3); each spectrum was normalized to the total N(1s) area.

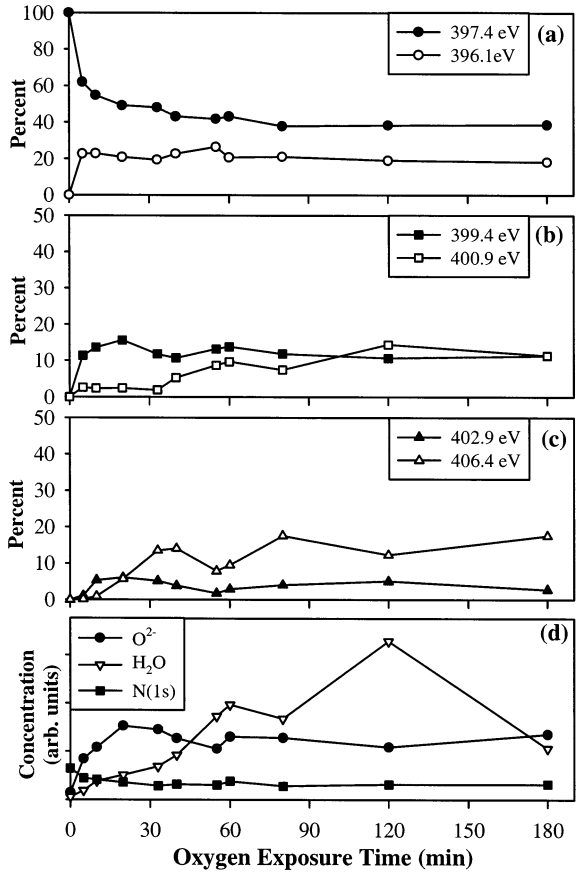

Figure 2. (a)−(c) Variation in the composition of the N(1s) region as a function of oxygen exposure time. Figure 2 shows the variation in XPS peak areas of the fitted peaks at (a) 397.4 eV (●) and 396.1 eV (○), (b) 399.4 eV (■) and 400.9 eV (□), (c) 402.9 eV(▲) and 406.4 eV (△). (d) This figure shows the variation in the elemental surface composition during low temperature exposure to oxygen, represented by the concentration of the O^{2-} (●) and H_2O (▽) peaks from the O(1s) region and the total N(1s) area (■). Data were collected from the same set of experiments shown in Figure 1.

to O_2^- and OH^-, the concentration of adsorbed H_2O grows linearly with exposure time, consistent with background water adsorption. During the initial period of oxidation, Figure 2d shows that the total N(1s) signal decreases by 50%, but within experimental error it remains constant for longer oxygen exposures. Although XPS data indicate that the iron oxide-(hydroxide) film thickness reaches a limiting value after ≈20 min, the distribution of nitrogen-containing species continues to evolve, evidenced by a comparison of Figure 2d and Figure 1 for oxygen exposure times >20 min.

Figure 3 shows the effects of X-ray irradiation on the N(1s) XPS region of a nitrided iron surface that was initially exposed to oxygen for 60 min with the substrate held at 113 K (Figure 3a), and subsequently irradiated by X-rays for 60 min (Figure 3b). Figure 3c shows the N(1s) difference spectra between Figure 3a and 3b, indicating that the 406.4 eV peak was depleted by X-ray irradiation. Figure 3d shows the XP spectra of an iron nitrate standard ($Fe(NO_3)_3$) showing a single peak located at ≈406.8 eV, proximate to the highest binding energy species observed in the N(1s) XPS region during oxidation.

Figure 4 shows the results from different experiments designed to probe the influence of temperature on the oxidation process. Figure 4a shows the effects of annealing an oxidized surface initially exposed to O/O_2 for 60 min at 125 K. Following low temperature oxidation (Figure 4a(i)), the N(1s) region can be well fitted by a combination of peaks centered at 406.4, 400.9, 399.4, and 396.1 eV, using the same fitting protocol employed in Figure 1. Upon annealing to 156 K (Figure 4a-(ii)), the 406.4 eV peak almost disappears, although this effect can be attributed to X-ray-induced decomposition during data acquisition (see Figure 3). At 173 K Figure 4a(iii), the peak at 400.9 eV in the N(1s) region decreases, coincident with an increase in the peak at 399.4 eV. Indeed, despite the change in the overall N(1s) envelope between 156 and 173 K, the sum of the N(1s) XPS areas associated with the peaks at 399.4 and 400.9 eV remains constant. Between 173 and 189 K, Figure 4a(iii) and (iv) shows that the N(1s) XPS envelope remained constant, while above 190 K (Figure 4a(v)) the intensity of the 396.1 and 399.4 eV peaks decreased, to leave a N(1s) envelope similar to that of the nitrided iron surface prior to oxidation (Figure 1a).

Figure 4b shows the variation in the N(1s) XPS region of nitrided iron surfaces initially exposed to oxygen at 125 K and then annealed to increasingly higher substrate temperatures under conditions where the undesirable effects of X-ray irradiation (see Figure 3) were minimized by using only 10 scans during XPS acquisition, instead of the 50−60 typically employed. The variation in the N(1s) spectra as a function of substrate temperature (Figure 4b) is similar to that in Figure 4a except that the 406.4 eV peak can still be resolved at 218 K. In contrast to Figure 4b, Figure 4c shows the variation in the N(1s) XPS region for three different experiments following exposure

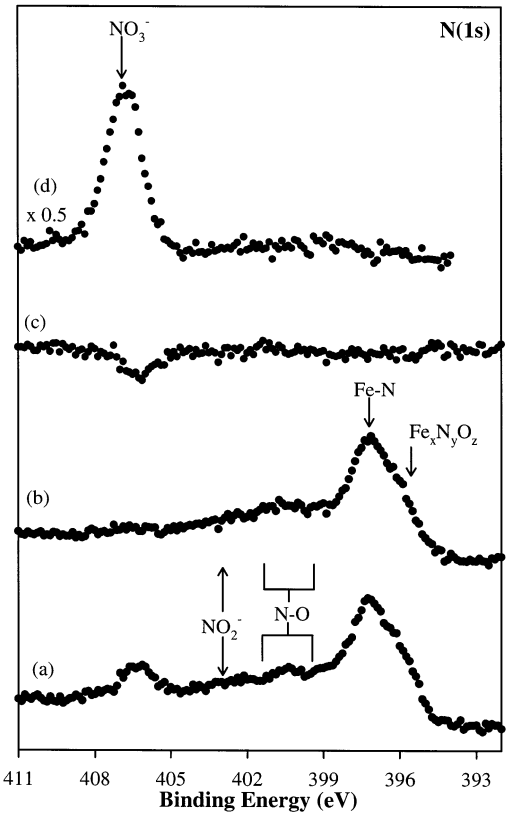

Figure 3. X-ray effects on the oxidized nitrided iron surface, observed in the N(1s) XPS region. (a) This figure shows the N(1s) spectra of the nitrided iron surface after 60 min exposure to oxygen at 113 K, while (b) shows the same surface after 60 min of X-ray irradiation. The sample temperature remained below 120 K during X-ray exposure. (c) This figure shows the N(1s) difference spectra between (b) and (a). (d) This figure shows the N(1s) XPS region of an iron nitrate ($Fe(NO_3)_3$) standard.

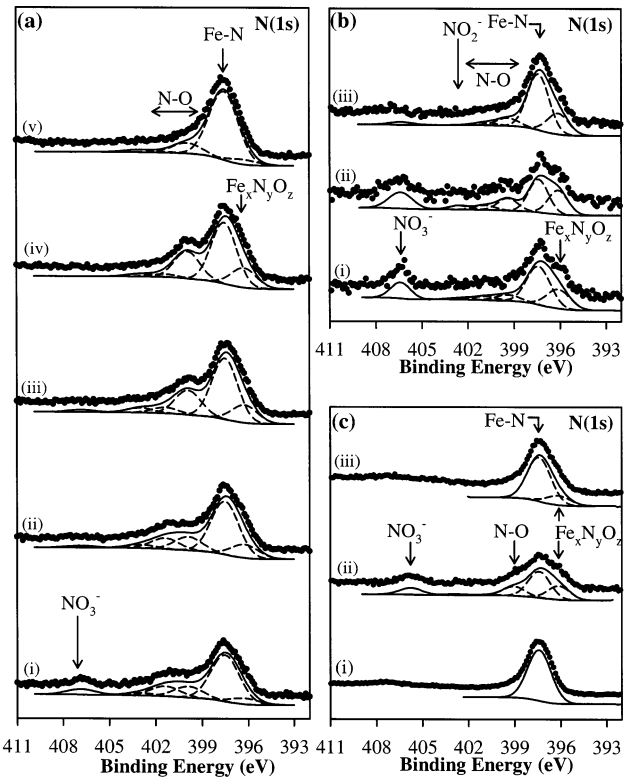

Figure 4. Influence of substrate temperature on the oxidized nitrided iron surface, as evidenced by the evolution of the N(1s) XPS region. The raw XPS data is shown as filled circles, peak fits as dashed lines, and envelopes and backgrounds as solid lines. Figure 4(a)(i) shows the N(1s) spectra of a nitrided iron overlayer after 60 min of oxygen exposure at 125 K (bottom spectra) and the effect of subsequent annealing to (ii) 156 K, (iii) 173 K, (iv) 189 K, and (v) 298 K. Figure 4(b)(i) shows the N(1s) spectra of a nitrided iron overlayer after 60 min of oxygen exposure at 125 K and the effect of subsequent annealing to (ii) 218 K and (iii) 298 K where the influence of X-ray irradiation was minimized (see text for details). Figure 4(c) shows the N(1s) spectra of a nitrided iron overlayer at (i) 125 K and after exposure to oxygen (with the substrate temperature maintained) at (ii) 189 K for 60 min and (iii) 298 K for 15 min.

of nitrided iron surfaces to oxygen at different substrate temperatures. Figure 4c(ii) illustrates that, at 189 K, new N(1s) features are observed at 396.1, 399.4, and 406.4 eV, while at 298 K (Figure 4c(iii)) the only new feature observed during oxidation is at 396.1 eV.

Figure 5 shows the evolution of the Fe(2p) and O(1s) XPS regions of a nitrided iron surface during exposure to oxygen at a substrate temperature of 125 K and following subsequent annealing. Before exposure to oxygen, the Fe(2p) region consisted of two peaks located at 706.8 and 719.9 eV corresponding to the $Fe(2p_{3/2})$ and $Fe(2p_{1/2})$ transitions of Fe/Fe_xN_y, respectively.[14,16] Upon oxidation, new peaks appeared in the Fe(2p) region centered at 710 and 723 eV indicative of iron oxide(hydroxide) production.[13,19] Prior to oxidation, the O(1s) XPS region exhibited no discernible spectral intensity. During exposure to oxygen, however, a broad peak appeared in the O(1s) region that was fitted to a combination of O^{2-} (≈530.0 eV), OH^- (≈532.1 eV), and H_2O (≈533.8 eV) species, the latter two a consequence of background water adsorption and decomposition.[20,21] With extended exposures (t > 60 min), all of the O(1s) peaks increased in intensity, although the H_2O peak became the dominant feature, indicating the buildup of a H_2O overlayer. No attempt was made to include peaks due to oxidized nitrogen N−O-containing species in the O(1s) region due to the relatively small concentration of nitrogen.

Upon annealing, changes in the O(1s) XPS region involved a steady decrease in the concentration of adsorbed water and an increase in the intensity of O^{2-} species, until by room temperature the O(1s) region is composed primarily of hydroxyl groups and oxide anions. Concomitant changes in the Fe(2p) region indicate an increase in the iron oxide thickness over this temperature range. Annealing of the oxidized surface to 814 K indicates that at these higher temperatures oxygen is lost from the overlayer, evidenced by changes in the O(1s) region and the Fe(2p) line shape, consistent with the formation of metallic iron at the surface.

The effect of adsorbed water on the oxidation process was examined explicitly by initially adsorbing ≈1 L of H_2O onto a nitrided iron surface at 117 K before annealing the surface to increasingly higher temperatures. The associated changes in both the N(1s) and O(1s) XPS regions are shown in Figure 6. Figure 6a shows that the O(1s) spectral envelope that develops during H_2O adsorption at 117 K is consistent with the presence of adsorbed H_2O, hydroxyl groups, and oxide anions. Concomitant changes in the N(1s) region during water adsorption were, however, less apparent than during oxygen exposure, with no evidence of any peaks in the N(1s) region at 396.1, 402.9, or 406.4 eV (compare Figure 1 and Figure 6). The N(1s) region was, however, observed to broaden to higher binding energies during H_2O adsorption at 117 K. Indeed, the resultant profile could be well-fitted by the inclusion of two new peaks centered at 399.4 and 400.9 eV, consistent with the position of new N(1s) peaks observed during oxygen exposure (Figure 1). The

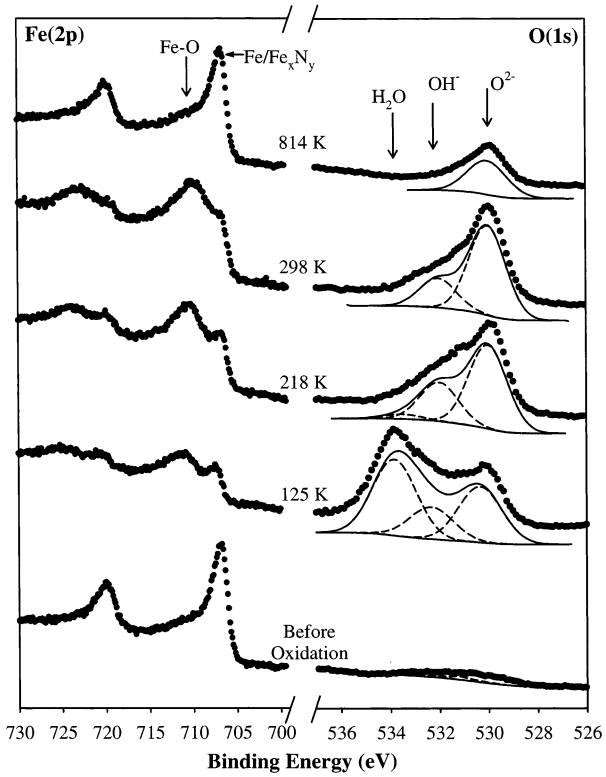

Figure 5. Influence of substrate temperature on the oxidized surface, monitored by the evolution of the Fe(2p) and O(1s) XPS regions. The nitrided iron surface was oxidized at 125 K for 55 min and subsequently annealed. The raw XPS data are shown as filled circles, peak fits as dashed lines, and envelopes and backgrounds as solid lines.

production of these new species is highlighted in the N(1s) difference spectra in Figure 6b, where the N(1s) XP spectra obtained after H_2O adsorption (and subsequent annealing) has had the N(1s) spectral envelope associated with the initial iron nitride subtracted. This analysis indicates that the appearance of new spectral intensity at ≈399 eV is coupled with the loss of parent nitride signal at 397.4 eV.

Figure 6 illustrates that upon annealing to 189 K, water had desorbed from the surface, although the presence of oxidized nitrogen species was still evident in the N(1s) difference spectra. Further increases in the surface temperature up to 298 K produced a slight decrease in OH^- peak area and an increase in the O^{2-} peak area. These changes in the O(1s) XPS region between 189 and 298 K were accompanied by a loss of oxidized nitrogen species evidenced by the decrease in spectral intensity between 399 and 402 eV. However, the N(1s) difference spectra indicate that the loss of these oxidized nitrogen species is not accompanied by any increase in the N(1s) intensity associated with the parent nitride.

Figure 7 shows the results of RAIRS experiments carried out in chamber-2 on a nitrided iron surface during exposure to oxygen at 117 K and subsequent annealing to 420 K. Figure 7 showed that oxidation was accompanied by the appearance of a new band centered at 2200 cm^{-1}. Upon annealing the surface above 200 K, the shape of the 2200 cm^{-1} band sharpened, while the spectral intensity of the band decreased over a broad temperature range between 200 and 420 K. Figure 7 (top spectra) also shows comparative RAIRS spectra obtained when $^{18}O/^{18}O_2$ was used to oxidize the nitrided iron surface at 117 K. Results from this experiment show that a new band is observed at ≈2060 cm^{-1} during $^{18}O/^{18}O_2$ exposure, in addition to the continued presence of a smaller peak centered at 2200 cm^{-1}. The inset in Figure 7 shows the N(1s) XP spectra of a nitrided iron substrate oxidized at 189 K in chamber-2. In addition to the presence of the parent iron nitride peak centered at ≈397.4 eV, spectral intensity in the N(1s) region is also observed between 400 and 402.5 eV. (It should be noted that the N(1s) XPS shown in Figure 7 was recorded at a lower resolution than Figures 1, 3−6 as a result of the poorer signal-to-noise ratio of the XPS system in chamber-2 compared to that in chamber-1.) In separate experiments using an MCT detector to probe the vibrational characteristics below 1900 cm^{-1}, no IR bands could be resolved.[22]

Figure 8 illustrates the results of mass spectrometry desorption experiments carried out in chamber-1 designed to identify the nature of volatile species produced during thermal annealing of an oxidized nitrided iron surface. The results in Figure 8 originate from two separate experiments where the nitrided iron surface was exposed to oxygen for 20 min at 125 K (a,b,e) and for 60 min at 117 K (c,d). Figure 8 shows that during sample annealing a broad multi-peak feature associated with NO (mass 30) desorption was detected between 210 and 440 K. In this temperature range, several peaks can be resolved within the NO desorption envelope. In contrast, no discernible intensity at masses (amu) 28 (N_2, CO), 44 (CO_2, N_2O), or 46 (NO_2) was observed between 210 and 440 K corresponding to the parent ion signal associated with other possible nitrogen-containing species. The sharp initial peak at mass 28 can be ascribed to background desorption of nitrogen from the copper rods. Similarly, the broad peak at 44 amu is ascribed to desorption of background CO_2. Any desorption of N_2O associated with this low temperature feature at mass 44 in Figure 8d can be excluded because of the absence of corresponding intensity at mass 30 (Figure 8c), since NO^+ is a significant cracking fragment of N_2O in the mass spectrometer.[23]

Discussion

Species Identification. Figures 1, 3, and 4 indicate that the reaction of oxygen with the nitrided iron surface under low temperature (<150 K) conditions produces a range of new nitrogen-containing species in addition to iron oxide/hydroxide (Figure 5). These species along with their XPS peak positions are listed in Table 1, and are assigned to oxynitride ($Fe_xN_yO_z$), $NO^+(1)$, $NO^+(2)$, NO_2^- (nitrito or nitrite), and nitrate (NO_3^-) species. In this section, the rationale for the different peak assignments in the N(1s) region are discussed in order of increasing N(1s) binding energy.

395−397 eV. In the present investigation, the presence of a distinct peak in the N(1s) XPS region at a lower binding energy (396.1 eV) than the parent nitride peak (397.4 eV) is most clearly observed in Figure 4b(i). A similar feature has been observed during oxidation of transition metal nitrides, including Ti,[8−10] Fe,[14] Cr,[8,9] and Zr,[9,11] and has been identified with the production of an oxynitride. This has been most clearly demonstrated in a XPS study of TiN dry-oxygen oxidation under vacuum conditions[10] where the appearance of a N(1s) peak shifted to ≈1 eV lower binding energy than the parent nitride, was accompanied the appearance of O^{2-} anions in the O(1s) region in the absence of TiO_2 or NO_x production, indicative of oxynitride formation. An oxynitride is characterized by the presence of both O^{2-} and N^{3-} anions distributed around the counter metal cation in a crystalline lattice.[24] The lower N(1s) binding energy of oxynitride relative to nitride has been rationalized by an increase in ionic character of the metal−oxygen bond, resulting in greater charge transfer from metal to nitrogen in the oxynitride.[8,10]

399−402 eV. A comparison of the N(1s) XP spectra and the RAIR spectra shown in Figure 7 reveals that the IR peak

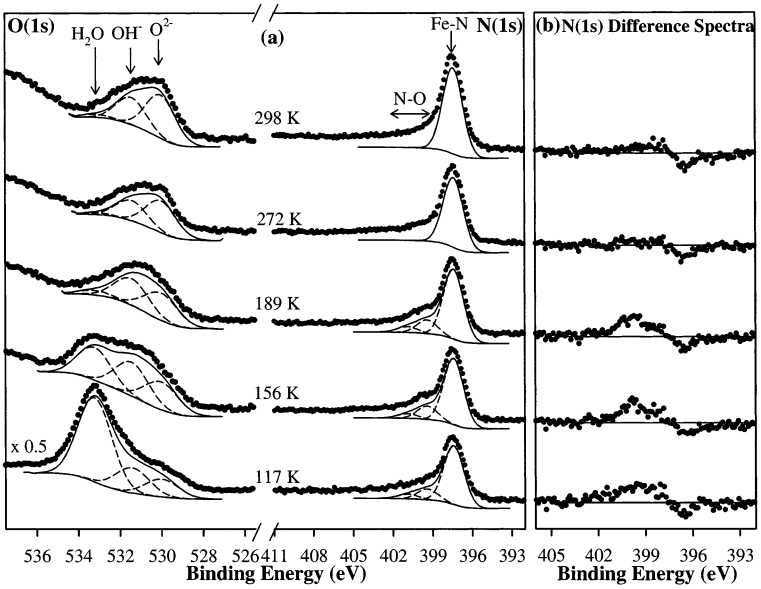

Figure 6. Influence of water on the oxidation of a nitrided iron surface. (a) This figure shows the O(1s) and N(1s) XPS regions after exposure to water at 117 K and then after the substrate was annealed to increasing temperatures, up to room temperature. (b) This figure shows the corresponding N(1s) difference spectra for each temperature relative to the initial N(1s) nitride peak. XPS spectra are shown in filled circles, fitted peaks in dashed lines, and envelopes and backgrounds in solid lines.

TABLE 1: Peak Parameters for the Fitted Peaks in the N(1s) XPS Region

Species	Binding Energy (eV)
oxynitride ($Fe_xN_yO_z$)	396.1
FeN	397.4
NO^+ (1)	399.4
NO^+ (2)	400.9
NO_2^-	402.9
NO_3^-	406.4

centered at ≈2200 cm^{-1} is correlated with those oxidized nitrogen species with binding energies between ≈399−402 eV. In related studies involving (NO + O_2) coadsorption on zeolite H-ZSM-5, IR bands at ≈ 2200 cm^{-1} have been assigned to nitrosonium ions (NO^+) bound to O^{2-} lattice anions, [29] within the 2390−2150 cm^{-1} range typically observed for the N−O stretch in nitrosonium salts.[30,31] In another related study by Liu et al.,[32] however, a 2125 cm^{-1} band was assigned to a N−N stretch within an Al−NN species. It should be noted that IR features associated with oxynitrides (i.e., metal−nitrogen and metal−oxygen stretches) give IR peaks at considerably lower frequencies (<1000 cm^{-1})[25−28] than the 2200 cm^{-1} peak position observed (Figure 7). In the present investigation, a comparison of RAIRS experiments using $^{16}O_2$ and $^{18}O_2$ supports the idea that the nitrogen species associated with the N(1s) peaks between 399 and 402 eV are due to the presence of NO^+ ions rather than N−N-containing moieties. Thus, Figure 7 illustrates that isotopic substitution experiments using $^{18}O_2$ produced a new band at 2060 cm^{-1}, red-shifted by 140 cm^{-1}, very close to the theoretical value expected for ^{18}O substitution in a N−O bond. Furthermore, the observed IR band position in Figure 7 coincides with the reported frequency (2200 cm^{-1}) of the N−O stretch in (NO)$FeCl_4$.[31,33] The higher IR peak position of the NO^+ band position relative to molecularly adsorbed NO (1870−1750 cm^{-1})[34−36] is a result of the loss of electron density from the π antibonding orbital resulting in an increase in the N−O bond order, blue-shifting the N−O stretching frequency in NO^+ into the range 2391−2102 cm^{-1}.[37]

Although the N(1s) feature at ≈399.4 eV can be assigned to the production of a NO^+ species, Figure 1 reveals that upon prolonged oxidation, the N(1s) spectral envelope in the 399−402 eV region broadens to higher binding energies, requiring the inclusion of another N(1s) feature with a peak centered at 400.9 eV. The exact identity of this feature is unclear, but the conversion of this species into nitrosonium ions during thermal annealing of the oxidized nitrided iron surface (Figure 4) suggests that these two species are chemically related. One possibility is that the peak centered at 400.9 eV corresponds to NO^+ ions interacting with water in addition to lattice oxygen anions. This assertion is based on the appearance of the 400.9 eV peak only after prolonged oxidation, when the buildup of H_2O at the surface becomes significant. Furthermore, annealing experiments on the oxidized surface show that the temperature at which the 400.9 eV peak converts to the peak at 399.4 eV corresponds to the temperature range where water desorbs (Figures 4, 5, and 6). Another possibility is that the 400.9 eV peak corresponds to NO^+ adsorbed on Fe^{2+}/Fe^{3+}, although no evidence was found for the associated N−O stretch, reported to lie between 1880 and 1820 cm^{-1}.[35,38,39]

402.5−403.5 eV. The peak at 402.9 eV, which is prominent during the early stages of oxidation, but becomes less significant as the oxidation process continues (Figure 1), is assigned to the formation of a nitrite (NO_2^-) or nitrito (−ONO) species.[40,41] The N(1s) peak position at 402.9 eV, however, also closely corresponds to the N(1s) binding energy due to the ***N***−NO associated with adsorbed N_2O. Adsorbed N_2O would, however, produce two N(1s) peaks of roughly equal intensity due to the ***N***−NO and N−***N***O species located at 402.7 and 406.4 eV,[42] inconsistent with our experimental observations (Figures 1 and 4). In addition, control experiments indicated that N_2O did not adsorb on the nitrided iron surface at 113 K.

Oxidation of Cr,[7,8] Ti,[8,9] and Zr[9,11] nitrides above 300 K has also been shown to produce a new peak in the N(1s) region between 402 and 403.2 eV ascribed to the formation of N_2 in either a metal−N−N−metal type structure[11,32] or simply N_2 adsorbed within the lattice.[7,9] In our present investigation, however, we do not believe that oxidation of the nitrided iron surface leads to the production of a N_2-type species. This assertion is based, in part, upon the absence of N_2 desorption during thermal annealing experiments (Figure 8). Furthermore,

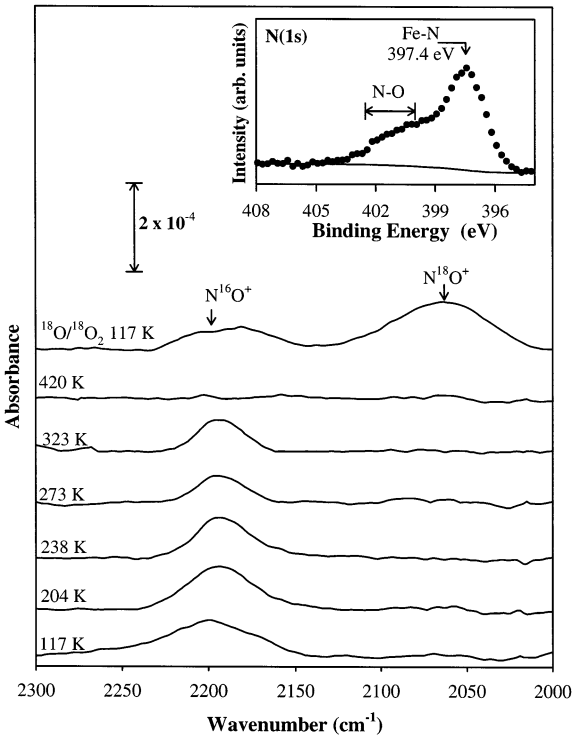

Figure 7. RAIRS spectra using an InSb detector showing the evolution of the spectral region from 2300 to 2000 cm^{-1} following exposure of the nitrided iron surface to oxygen with the substrate initially held at 117 K and then annealed to increasingly higher temperatures. The uppermost RAIRS spectrum corresponds to a separate experiment where the nitrided iron surface was oxidized at ≈120 K for 60 min using $^{18}O/^{18}O_2$. The inset shows the N(1s) XP spectra of a nitrided iron surface oxidized at 189 K.

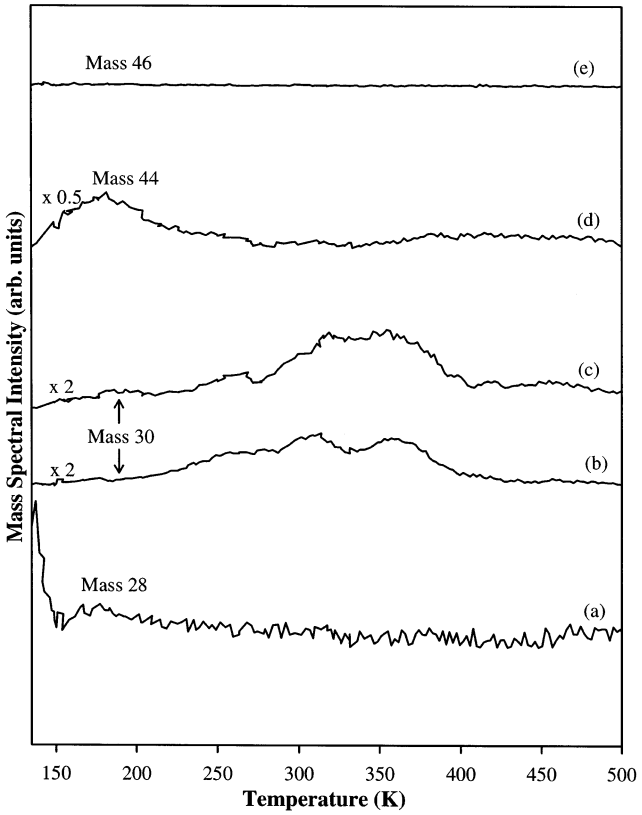

Figure 8. Mass spectrum of volatile species produced during annealing of nitrided surfaces following exposure to oxygen (temperature ramp ≈ 3 K/s). Figure 8 shows the mass spectrum intensity at (a) mass 28 (N_2 and CO), (b) and (c) mass 30 (NO), (d) mass 44 (CO_2, N_2O), and (e) mass 46 (N_2O) amu as a function of substrate temperature. (a), (b), and (e) were obtained for nitrided iron surfaces initially exposed to oxygen for 20 min with the substrate held at 125 K, while (c) and (d) were collected following 60 min of oxygen exposure (substrate temperature 117 K).

the 402.9 eV peak passes through a maximum during the early stages of oxidation attenuating at longer O/O_2 exposures (Figure 1). This observed behavior associated with the peak at 402.9 eV is characteristic of an intermediate species, arguing against the assignment of this peak to N_2, since no N_2-type species are expected to act as an intermediate in the oxidation process.

406−407 eV. The peak observed at 406.4 eV, corresponding to a highly oxidized nitrogen moiety becomes increasingly prominent upon prolonged oxygen exposure (Figure 1). This feature is identified with a nitrate (NO_3^-) species based on previous literature assignments[40,43] and a comparison with the N(1s) peak recorded from the $Fe(NO_3)_3$ standard (Figure 3). Although N(1s) peaks at 406.4 eV have also been ascribed to the N−*N*O species in adsorbed N_2O,[42] the absence of a 1:1 area intensity ratio and the lack of positive correlation between the peaks at 406.4 and 402.9 eV indicates that N_2O is not produced. Furthermore, only the peak at 406.4 eV is degraded under the influence of X-ray irradiation (Figure 3), consistent with the susceptibility of nitrate species to electron-stimulated decomposition[44] and to the observed instability of the $Fe(NO_3)_3$ standard under the influence of X-ray irradiation.

Dynamics of Oxidation. Figure 1 illustrates that during the initial stages of oxidation, the dominant process involves the production of iron oxynitride ($Fe_xN_yO_z$) and the formation of nitrosonium ions (NO^+) and iron oxide(hydroxide) (the latter evidenced by changes in the Fe(2p) region). Focusing on the nitrogen-containing species, the overall process can be represented schematically (Scheme 1).

Indeed, a number of previous studies on the high temperature (≥300 K) oxidation of transition metal nitrides under ambient conditions indicate the simultaneous formation of peaks in the

SCHEME 1: Nitrosonium ion and iron oxynitride

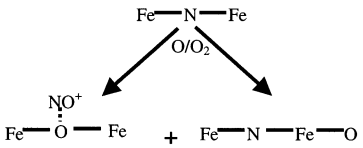

N(1s) region located at slightly higher and lower binding energies than the parent nitride peak, consistent with the production of bound N−O species as well as oxynitrides.[9,10,12−14] For example, Milosev et al.[9,12,45] have observed the formation of peaks at 396 and 400 eV in the N(1s) XPS region during the electrochemical oxidation of ZrN and TiN films. The idea that nitrosonium formation is an important reaction pathway in nitride oxidation is also supported by a previous diffuse reflectance infrared Fourier transform spectroscopy (DRIFTS) study where an intense peak at 2198 cm^{-1} (see Figure 7) was observed during the thermal oxidation of zirconium nitride.[11]

In the present investigation, oxidation of a nitrided iron surface subsequently annealed to 189 K in chamber-1 led to oxynitride and nitrosonium ion formation (Figure 4a(iv)) while the same experiment carried out in chamber-2 produced only nitrosonium ions (inset Figure 7). Cocke et al.[13] showed that air oxidation of plasma-nitrided iron produces an oxidized nitrogen species whose peak position is consistent with the production of an N−O-type species. In contrast, Graat et al.,[14] in a study of the air oxidation of ϵ-Fe_2N_{1-x}, observed a new N(1s) peak at lower binding energies than the parent nitride

peak, indicative of iron oxynitride formation. In conjunction, these results suggest that the nature of the nitrogen-containing species produced during oxidation is extremely sensitive to the detailed experimental conditions.

In contrast to previous studies detailing the oxidation of Cr,[7,8] Ti,[8] and Zr[11] nitrides, no N_2 was observed during the present study on iron nitride oxidation. One possible explanation for the lack of N_2 production may be the chemical composition of the iron nitride phase. Based on a literature survey, the dominant iron nitride produced as a result of N_2^+ and N^+ ion implantation is likely to be $Fe_{16}N_2$.[16] Given the low concentration of nitrogen atoms in $Fe_{16}N_2$, the probability of bimolecular reactions between two N atoms during oxidation is expected to be low, consistent with the absence of N_2 in the present investigation.

Figure 1 showed that after prolonged oxygen exposure at low temperatures (<150 K), the formation of nitrate-like species becomes significant. Indeed, after 180 min of oxygen exposure, nitrate species account for ≈20% of the N(1s) XPS signal (Figure 1 and Figure 2c). We propose that the formation of nitrate species occurs via the nitrite/nitrito-like intermediate. This assertion is based upon the presence of nitrite- or nitrito (NO_2^-)-type species, evidenced by the peak at 402.9 eV, at short oxygen exposures preceding the formation of NO_3^- and the induction period required before NO_3^- ions are observed (Figure 1 and Figure 2c). This overall oxidation process is postulated to proceed through the insertion of oxygen into Fe−N bonds and can be illustrated schematically (Scheme 2).

SCHEME 2: Nitrite/nitrito and nitrate formation

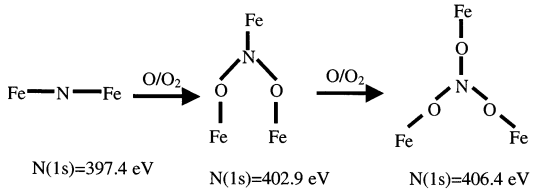

Interestingly, Figure 2c,d shows that the concentration of NO_3^- species continues to increase after the O_2^- and OH^- XPS signals attain their maximum values. This indicates that the oxidation of nitrogen-containing species continues even after the thickness of the iron oxide(hydroxide) film has reached a limiting value.

The idea that nitrite- or nitrito-like species can act as precursors for nitrate formation has been proposed in a recent study on the adsorption of NO/NO_2 on barium oxide [40] and has also been observed during the reaction of NO and O_2 with $Pt/BaO/Al_2O_3$ catalysts.[46] Although the production of highly oxidized nitrogen species has been observed previously in adsorption studies of NO_x on oxide surfaces,[40,47−49] this investigation is the first to report their production during nitride oxidation. Furthermore, the observation of nitrate ions and nitrite-like species during oxygen exposure to iron nitride is of technological significance since these species are known to inhibit the anodic dissolution of iron.[50]

During oxygen exposure, the initial changes in the Fe(2p), O(1s), and N(1s) regions are consistent with the formation of iron oxide(hydroxide) whose presence is responsible for the decrease in the integrated N(1s) XPS area (Figure 2d). During this initial period of oxidation, nitrogen is partitioned primarily into iron oxynitride ($Fe_xN_yO_z$) or adsorbed nitrosonium ions (NO^+), the latter presumably arising from reactions associated with nitrogen atoms that have been displaced from the iron nitride lattice. Once formed, Figure 1 indicates that the iron oxynitride and adsorbed nitrosonium ions are stable. Thus, there does not appear to be any correlation between the formation of NO^+ and NO_3^- ions that would be consistent with the formation of nitrosonium nitrate ($NO_3^-NO^+$). An additional reaction pathway during oxidation involves the formation of nitrite/nitrito species as a result of oxygen insertion into the iron nitride lattice (Scheme 2). Upon prolonged oxygen exposure, nitrate ions are observed as a result of further oxygen incorporation into the overlayer, although by this time the thickness of the iron oxide-(hydroxide) layer formed at the vacuum/substrate interface has reached its limiting value. Our experimental results also suggest that nitrogen desorption is not a significant process under our low temperature (<150 K) oxidation conditions; thus, for oxygen exposures in excess of 20−30 min, the total N(1s) XPS area remains constant, despite continued changes in the distribution of oxidized nitrogen species (Figure 2).

Figure 1 also shows that a significant fraction of the parent nitride remains intact during the oxidation process. This can be attributed to the fact that the thickness of the nitrided overlayer synthesized using high-energy (3 keV) ion implantation (≈10 nm)[16] is greater than the penetration both of molecular or atomic oxygen within the nitrided iron overlayer at ≈150 K. As noted by previous authors,[8] the limited penetration depth of oxygen also results in a gradient of oxygen concentration below the oxidized nitride surface. In the context of the present investigation, the topmost surface layers are expected to consist principally of iron oxide(hydroxide) while the various oxidized nitrogen-containing species (e.g., nitrates and oxynitrides) are concentrated between this iron oxide(hydroxide) surface layer and the deeper-lying nitrided iron. This assertion was corroborated by related experiments, where an oxidized sample whose initial N(1s) XP spectrum resembled that shown in the inset to Figure 7 was bombarded with Ar^+ (3 keV). Subsequent XPS analysis following ion bombardment revealed that the relative concentration of oxidized nitrogen species was depleted, confirming that the N−O species were concentrated closer to the substrate/vacuum interface compared to the underlying nitride.

The thickness of the oxidized overlayer during various stages of the low-temperature oxidation process and subsequent annealing has been calculated from the attenuation of the iron nitride N(1s) peak (Figure 1). Results form this analysis reveal that after 60 min of oxygen exposure, the thickness of the oxidized overlayer (containing iron oxide (hydroxide), adsorbed water as well as the various oxidized nitrogen species) is ≈2.5 nm. Upon annealing the surface to room temperature (Figure 4a(v)), the desorption of water and the loss of the various oxidized nitrogen species produces an iron oxide(hydroxide) film that is ≈2.0 nm thick on top of the residual nitrided iron layer.

Influence of Water in the Oxidation Process. The influence of H_2O on the oxidation of nitrided iron films is considered explicitly in Figure 6. On the basis of the N(1s) peak assignments, the evolution of the N(1s) region during H_2O adsorption onto the nitrided iron surface at 117 K (shown in Figure 6) is consistent with the idea that H_2O adsorption leads to the formation of iron oxide (hydroxide) and the production of N−O species, presumably adsorbed nitrosonium ions. The idea that reactions of $H_2{}^{16}O$ with the nitrided iron surface can lead to the production of nitrosonium ions is also consistent with the persistence of an IR band at 2200 cm^{-1} in Figure 7 associated with a $N-{}^{16}O$ linkage during low temperature reactions with $^{18}O_2$ in the absence of detectable $^{16}O_2$, presumably as a result of reactions with background $H_2{}^{16}O$.

Upon annealing to room temperature, the N(1s) difference spectra reveal that the spectral intensity at ≈399 eV, associated with oxidized nitrogen species, is lost without any increase in the parent nitride N(1s) signal. This observation suggests that these species desorb from the surface as volatile oxygen containing nitrogen moieties, supporting the hypothesis that the spectral intensity at ≈399 eV corresponds to distinct nitrogen-containing oxygen species produced during the H_2O oxidation process.

In contrast to oxygen exposure, water exhibits considerably less oxidizing power, evidenced by the absence of nitrites, nitrates, or oxynitride species (compare Figure 6 and Figure 1). The weaker oxidizing power of water on iron surfaces is also consistent with studies by Bernasek et al. on iron oxidation by H_2O and O_2.[51] It should also be noted that the nature of the reaction products observed during oxygen exposure to the nitrided iron surface are similar at surface temperatures above and below the desorption temperature of water. Thus, Figures 1 and 4(c) indicate that the formation of NO_3^-, NO^+, and oxynitride species are observed during exposure of the nitrided iron surface to oxygen at 150 and 189 K, indicating that the distribution of nitrogen-containing products is largely unaffected by the presence of adsorbed water. It is possible however, that the buildup of an adsorbed water layer at low temperatures may act to limit the extent of oxidation for prolonged oxygen exposures.

Thermal Stability of the Oxidized Overlayer. Thermal desorption experiments (Figure 8) indicate that in the temperature regime below 500 K, nitrogen is lost from the surface over a fairly broad temperature range (220−400 K) exclusively as NO, evidenced by a desorption peak at 30 amu (NO^+) coupled with the lack of any spectral intensity over this temperature range associated with N_2, N_2O, or NO_2. The onset of NO desorption above 200 K is also consistent with XPS (Figures 4 and 6) and RAIRS measurements (Figure 7). Furthermore, the fact that no XPS evidence is found for N_2O production during oxygen exposure and that changes in the N(1s) region following oxygen exposure occur at temperatures above ≈220 K support the idea that the 44 amu peak (Figure 8) observed between 150 and 200 K is due to CO_2 rather than N_2O desorption. NO desorption is primarily ascribed to the loss of NO^+ species from the surface as well as the decomposition of nitrate and nitrite/nitrito moieties. Indeed, the fact that the NO desorption profile is broad (Figure 8), exhibiting more than one peak within the desorption envelope, is consistent with the idea that a variety of species contribute to the loss of NO from the surface. The decomposition of the highly oxidized nitrogen species (nitrate or nitrite/nitrito species) between 220 and 298 K is reflected by the absence of nitrate species following room-temperature oxidation, shown in Figure 4c. Thermal decomposition of nitrate and nitrite/nitrito species to NO and adsorbed oxygen is also believed to be responsible for the modest increase in the iron oxide film thickness (evidenced in Figure 5 by changes in the Fe(2p) region) during annealing of the oxidized film above 200 K.

At substrate temperatures above ≈520 K, the N(1s), O(1s), and Fe(2p) envelopes indicate that the film structure is composed only of an iron oxide(hydroxide) layer on top of nitrided iron. No spectral intensity associated with N−O species, nitrates, nitrite/nitrito, or iron oxynitrides remains. It is highly plausible and chemically reasonable that the thermal decomposition of adsorbed nitrosonium ions, nitrite/nitrito, and nitrate species leads to the evolution of NO. In contrast, we believe that iron oxynitride ($Fe_xN_yO_z$) will phase segregate into iron oxide and iron nitride upon heating, similar to previous studies on the thermal decomposition of titanium oxynitride.[10] Once formed, the iron oxide(hydroxide) and nitrided iron layers remain stable until ≈650 K. Above 650 K, nitrogen and oxygen are both lost from the surface, evidenced by changes in the O(1s) and N(1s) XPS regions and the line shape of the Fe(2p) peaks, indicative of a return to metallic Fe character (Figure 5). This observation is in agreement with previous studies on the thermal stability of iron oxide surface films and adsorbed nitrogen under vacuum conditions.[52]

Conclusions

During the initial exposure of a nitrided iron film to oxygen at low temperatures (<150 K), the dominant new nitrogen-containing species produced are iron oxynitride and nitrosonium ions. The production of nitrosonium ions was confirmed by $^{18}O_2$ isotopic labeling experiments. Upon prolonged oxygen exposure, highly oxidized nitrate (NO_3^-) species are also observed due to the oxidation of a nitrite (NO_2^-) or nitrito-like intermediate. In separate experiments, water was found to exhibit considerably less oxidizing power than oxygen, producing only adsorbed N−O species. Experiments on the thermal stability of the oxidized nitride overlayer revealed that nitrogen is lost from the surface as NO above ≈210 K, resulting in a near-surface region composed of iron oxide(hydroxide) and unreacted nitrided iron that remained stable until ≈650 K. By carrying out nitride oxidation at low temperatures, an additional reaction pathway associated with oxidation has also been identified, specifically, oxygen insertion into the Fe−N lattice, ultimately leading to the production of nitrate ions.

Acknowledgment. Partial support for this research was provided by a grant from the Petroleum Research Fund (PRF # 35281 - G5, G6) administered through the American Chemical Society.

References and Notes

(1) Santhanam, A. T. Application of transition metal carbides and nitrides in industrial tools. In *Chemistry of transition metal carbides and nitrides*; Oyama, S. T., Ed.; Blackie: Glasgow, 1996; p 28.
(2) Narula, C. K. *Ceramic Precursor Technology and its Applications*; Marcel Dekker: New York, 1995.
(3) Hubler, R.; Cozza, A.; Marcondes, T. L.; Souza, R. B.; Fiori, F. F. *Surf. Coat. Technol.* **2001**, *142*, 1078.
(4) Stroemme, M.; Karmhag, R.; Ribbing, C. G. *Opt. Mater.* **1995**, *4*, 629.
(5) Holleck, H. *J. Vac. Sci. Technol. A* **1986**, *4*, 2661.
(6) Kim, S. H.; Chung, D. S.; Park, K. C.; Kim, K. B.; Min, S. H. *J. Electrochem. Soc.* **1999**, *146*, 1455.
(7) Esaka, F.; Shimada, H.; Imamura, M.; Matsubayashi, N.; Sato, T.; Nishijima, A.; Kawana, A.; Ichimura, H.; Kikuchi, T.; Furuya, K. *Thin Solid Films* **1996**, *282*, 314.
(8) Esaka, F.; Furuya, K.; Shimada, H.; Imamura, M.; Matsubayashi, N.; Sato, T.; Nishijima, A.; Kawana, A.; Ichimura, H.; Kikuchi, T. *J. Vac. Sci. Technol. A* **1997**, *15*, 2521.
(9) Milosev, I.; Strehblow, H. H.; Navinsek, B. *Thin Solid Films* **1997**, *303*, 246.
(10) Prieto, P.; Kirbi, R. E. *J. Vac. Sci. Technol. A* **1995**, *13*, 2819.
(11) Wiame, H.; Centeno, M. A.; Picard, S.; Bastians, P.; Grange, P. *J. Eur. Ceram. Soc.* **1998**, *18*, 1293.
(12) Milosev, I.; Strehblow, H. H.; Gaberscek, M.; Navinsek, B. *Surf. Interface Anal.* **1996**, *24*, 448.
(13) Cocke, D. L.; Jurcik-Rajman, M.; Veprek, S. *J. Electrochem. Soc.* **1989**, *136*, 3655.
(14) Graat, P. C. J.; Somers, M. A. J.; Mittemeijer, E. J. *Appl. Surf. Sci.* **1998**, *136*, 238.
(15) Carlo, S. R.; Torres, J.; Fairbrother, D. H. *J. Phys. Chem. B* **2001**, *105*, 6148.
(16) Sanghera, H. K.; Sullivan, J. L. *Nucl. Instrum. Methods Phys. Res. B* **1999**, *152*, 65.
(17) Torres, J.; Perry, C. C.; Bransfield, S. J.; Fairbrother, D. H. *J. Phys. Chem. B* **2002**, *106*, 6265.

(18) Diekmann, W.; Panzner, G.; Grabke, H. J. *Surf. Sci.* **1989**, *218*, 507.
(19) *The Handbook of XPS Spectroscopy*; Wagner, C. D., Riggs, W. M., Davis, L. E., Moulder, J. F., Muilenberg, G. E., Eds.; Perkin-Elmer Corporation: Eden Praire, MN, 1979.
(20) Clarke, N. S.; Hall, P. G. *Langmuir* **1991**, *7*, 678.
(21) Debnath, N. C.; Anderson, A. B. *Surf. Sci.* **1983**, *128*, 61.
(22) The lack of IR signal during experiments using an MCT detector can be ascribed to significantly lower signal-to-noise ratio compared to InSb detectors.
(23) From the Balzers Mass Spectrum database $N_2O^+(44):NO^+(30) = 100:31$.
(24) Clarke, S. J.; Michie, C. W.; Rosseinsky, M. J. *J. Solid State Chem.* **1999**, *146*, 399.
(25) Naiman, M. L.; Kirk, C. T.; Emerson, B. L.; Taitel, J. B. *J. Appl. Phys.* **1985**, *58*, 779.
(26) Diniz, J. A.; Tatsch, P. J.; Pudenzi, M. A. A. *Appl. Phys. Lett.* **1996**, *69*, 2214.
(27) Kim, J. Y.; Sriram, M. A.; McMichael, P. H.; Kumta, P. N.; Phillips, B. L.; Risbud, S. H. *J. Phys. Chem. B* **1997**, *101*, 4689.
(28) Ono, H.; Ikarashi, T.; Miura, Y.; Hasegawa, E.; Ando, K.; Kitano, T. *Appl. Phys. Lett.* **1999**, *74*, 203.
(29) Hadjiivanov, K.; Saussey, J.; Freysz, J. L.; Lavalley, J. C. *Catal. Lett.* **1998**, *52*, 103.
(30) Nakamoto, K. *Infrared Spectra of Inorganic and Coordination Compounds*; Mir: Moscow, 1966.
(31) Laane, J.; Ohlsen, J. R. *Prog. Inorg. Chem.* **1986**, *27*, 465.
(32) Liu, H.; Bertolet, D. C.; Rogers, J. W. *Surf. Sci.* **1995**, *340*, 88.
(33) Sharp, D. W. A.; Thorley, J. *J. Chem. Soc.* **1986**, 3557.
(34) Aparicio, L. M.; Hall, W. K.; Fang, S. M.; Ulla, M. A.; Millman, W. S.; Dumesic, J. A. *J. Catal.* **1987**, *108*, 233.
(35) Fabrizioli, P.; Burgi, T.; Baiker, A. *J. Catal.* **2002**, *206*, 143.
(36) Yuen, S.; Chen, Y.; Kubsh, J. E.; Dumesic, J. A.; Topsoe, N.; Topsoe, H. *J. Phys. Chem.* **1982**, *86*, 3022.
(37) Hadjiivanov, K. I. *Catal. Rev.—Sci. Eng.* **2000**, *42*, 71.
(38) Chen, H. Y.; Voskoboinikov, T.; Sachtler, W. M. H. *J. Catal.* **1998**, *180*, 171.
(39) Hadjiivanov, K.; Knözinger, H.; Tsyntsarski, B.; Dimitrov, L. *Catal. Lett.* **1999**, *62*, 35.
(40) Schmitz, P. J.; Baird, R. J. *J. Phys. Chem. B* **2002**, *106*, 4172.
(41) Lin, J.; Wee, A. T. S.; Tan, K. L. *Inorg. Chem.* **1993**, *32*, 5522.
(42) Baldwin, E. K.; Friend, C. M. *J. Vac. Sci. Technol. A* **1986**, *4*, 1407.
(43) Honda, F.; Hirokawa, K. *J. Electron. Spectrosc. Relat. Phenom.* **1976**, *8*, 199.
(44) Petrik, N. G.; Knutsen, K.; Paparazzo, E.; Lea, S.; Camaioni, D. M.; Orlando, T. M. *J. Phys. Chem. B* **2000**, *104*, 1563.
(45) Milosev, I.; Srehblow, H. H.; Navinsek, B. *Surf. Interface Anal.* **1998**, *26*, 242.
(46) Westerberg, B.; Fridell, E. *J. Mol. Catal. A*: *Chem.* **2001**, *165*, 249.
(47) Hadjiivanov, K.; Buschev, V.; Kantcheva, M.; Klissurski, D. *Langmuir* **1994**, *10*, 464.
(48) Hadjiivanov, K.; Knözinger, H. *Phys. Chem. Chem. Phys.* **2000**, *2*, 2803.
(49) Kantcheva, M. *J. Catal.* **2001**, *204*, 479.
(50) Gabrielli, C.; Keddam, M.; Stupnisek-Lisac, E.; Takenouti, H. *Electrochim. Acta* **1976**, *21*, 757.
(51) Hung, W. H.; Schwartz, J.; Bernasek, S. L. *Surf. Sci.* **1993**, *294*, 21.
(52) Honda, F.; Hirokawa, K. *Talanta* **1978**, *25*, 383.